Available online at www.sciencedirect.com
ScienceDirect
Ceramics International 36 (2010) 1245–1251
CERAMICS INTERNATIONAL
www.elsevier.com/locate/ceramint

Preparation and characterizations of highly transparent UV-curable ZnO-acrylic nanocomposites

Heh-Chang Huang, Tsung-Eong Hsieh *

Department of Materials Science and Engineering, National Chiao Tung University, 1001 Ta-Hsueh Road, Hsinchu 30010, Taiwan, ROC

Received 23 October 2009; received in revised form 23 November 2009; accepted 18 December 2009
Available online 28 January 2010

Abstract

A sol–gel chemical route was adopted to prepare the zinc oxide (ZnO) nanoparticles as small as 4 nm. UV-curable ZnO-acrylic nanocomposites were then prepared by employing 3-(trimethoxysilyl)propyl methacrylate (TPMA) as the surface modification agent of ZnO particles. UV–vis analysis revealed a high optical transparency (>95%) in visible light region for nanocomposite thin films with ZnO contents up to 20 wt.%. The addition of ZnO nanoparticles also enhanced the dielectric constants of nanocomposites and the dielectric constants greater than 4 in frequencies ranging from 1 to 600 MHz was obtained in the samples containing 10 wt.% of ZnO nanoparticles. A comparison of experimental results and theoretical calculation indicated that the interfacial polarizations in between ZnO nanoparticles and polymer matrix may play an important role in the enhancement of dielectric properties of nanocomposites.

Keywords: B. Nanocomposites; C. Optical properties; C. Dielectric properties; D. ZnO

1. Introduction

In recent years, organic–inorganic nanocomposites attract a lot of research interests due to their versatility on thermal [1], electrical [2,3] and optical properties [4]. Among these, transparent nanocomposites possessing high refractive index (n ~1.65–1.79) [5] and high transparency in visible light region (transmittance > 90%) [6] are popular materials for the fabrication of optical fibers, waveguides, lenses and LED packages. In order to preserve the transparency, a uniform dispersion of nano-scale fillers in polymeric matrix and good interfacial compatibility between inorganic and organic components of nanocomposites are essential. Stelzig et al. utilized the surface active amphiphilic copolymers to trap the polar nanoparticle in a miscible multi-component solvent system so as to yield the highly transparent nanocomposites [7]. Althues et al. reported a surface functionalized nanoparticle with acrylic acid that can be added in the methyl methacrylate (MMA) monomer to prepare the transparent nanocomposites [8]. Previous studies also indicated that the utilization of homogeneous solutions comprised of nanoparticles and monomer is the most efficient way to prepare the transparent nanocomposites [6,7].

Most of the studies relating to transparent nanocomposites focused on the optical applications. For instance, transparent ZnS:Mn-poly(methyl methacrylate) (PMMA) nanocomposites prepared by Althues et al. exhibited high quantum yield (~29.8%) and transmittance (~87%) [8]. Lu et al. reported the PbS-polythiourethane (PTU) nanocomposites with high refractive index (n ~1.57–2.06) [9]. Transparent ZnO-epoxy nanocomposites have been prepared by Yang et al. and applied to the encapsulation of solid-state lighting devices [10]. Highly transparent photo-curable co-polyacrylate/silica nanocomposites were also used for the direct encapsulation of organic light emitting devices (OLEDs) [11].

In recent years, the demands of compactness and portability of electronic devices accelerate the development of flexible electronics in various aspects such as organic thin-film transistors (OTFTs) [12], organic solar cells (OSCs) [13], *etc*. Fabrication of flexible electronics always requires low-temperature processes and the UV-curable materials as well as

* Corresponding author. Tel.: +886 3 5712121x55306; fax: +886 3 5724727.
E-mail address: tehsieh@mail.nctu.edu.tw (T.-E. Hsieh).

0272-8842/$36.00
doi:10.1016/j.ceramint.2010.01.010

the processing methods are always the primary choices to fulfill such a requirement.

Zinc oxide (ZnO) is a well known optoelectronic material for its wide direct band gap (E_g = 3.25–3.5 eV) and large exciton binding energy (59 meV) which may provide the highly efficient exciton emission at room temperature [14,15]. Various processing methods, *e.g.*, sol–gel [16,17] and molecular capping [18,19], have been employed to form finely dispersed nano-scale ZnO particles in either organic or inorganic matrix. Distinct luminescence properties of those ZnO-relating nanocomposite systems and their relationships with defect structure and transition mechanisms have been reported [20–22]. This study employs a wet chemical route to synthesize the ZnO nanoparticles followed by a surface modification utilizing the 3-(trimethoxysilyl)propyl methacrylate (TPMA). The TPMA serves as not only the compatibility promoter between the ZnO and monomer, but also the dispersant agent of ZnO nanoparticles in the UV-curable transparent nanocomposites. The synthesis route of nano-scale ZnO particles and characterizations of microstructure, optical and electrical properties of nanocomposite samples are presented as follows.

2. Experiment

2.1. Materials

Zinc acetate dihydrate ($Zn(Ac)_2{\cdot}2H_2O$, purity = 99.6%) was purchased from J.T. Baker, Ltd. Absolute ethanol (purity = 99.5%) and methyl methacrylate (purity = 99%) were purchased from Fluka, Ltd. Lithium hydroxide monohydrate ($LiOH{\cdot}H_2O$, purity = 99%) was purchased from TEDIA. TPMA (purity = 98%) was purchased from Aldrich. 2-Hydroxyethyl methacrylate (HEMA, purity = 98%) was purchased from Acros. Ltd. Hexane (purity = 95%) was purchased from Seedchem, Ltd. Trimethylolpropane triacrylate (TMPTA, purity = 98%) and photoinitiator (chemcure 481) were purchased from Chembridge, Ltd. All reagents were directly used without further purification.

2.2. Preparation of ZnO nanoparticles

Preparation of ZnO nanoparticles and its modifications have been reported elsewhere [23,24]. In a typical run, 2.2 g of $Zn(Ac)_2{\cdot}2H_2O$ was first dissolved in 150 ml boiling ethanol, refluxed at 80 °C in argon ambient, and then held at this temperature for 3 h under vigorous stirring. During this process, 90 ml of ethanol was removed by distillation. After cooling above mixture down to 0 °C, a 90 ml of 0.58 g $LiOH{\cdot}H_2O$ in ethanol solution was added into the mixture under vigorous stirring. The stock solution was stirred continuously at room temperature for another 2 h until the mixed solution became transparent. By adding 300 ml of hexane, nano-scale ZnO particles were obtained and the supernatant was removed by centrifugation. 50 ml of ethanol was added into ZnO nanoparticles to re-suspend the nanoparticles in ethanol.

2.3. Surface modification of ZnO nanoparticles

Surface modification of ZnO nanoparticles was achieved as follows. 0.5 ml TPMA in 5 ml ethanol solution was added into the 150 ml as-synthesized ZnO nanoparticles in ethanol solution at 0 °C and then a reaction for 2 h was allowed. Afterward, the mixture was stirred at room temperature for 24 h. After adding the hexane, the TPMA-modified ZnO nanoparticles were obtained by centrifugally removing the supernatant.

2.4. Preparation of transparent UV-curable acrylic-ZnO nanocomposites

Various amounts of TPMA-modified ZnO nanoparticles in ethanol (2 ml) were blended with the monomers including MMA (0.9011 g; 0.009 mole), HEMA (1.9521 g; 0.015 mole), TMPTA (1.77792 g; 0.006 mole) and chemcure 481 photoinitiator (0.18546 g; 4 *wt.*%). The mixtures were stirred at room temperature for 24 h in argon ambient. The ethanol was then removed by reduced pressure distillation to form the resin precursor of ZnO nanocomposites. The nanocomposite precursor was coated on a polyester (PET) mold and cured by UV irradiation to form the nanocomposite samples with film thickness about 300 μm. The photo-polymerization was carried out in an UV oven (C-SUN CU1000, Taiwan) with principal wavelength = 365 nm, curing power = 80 W and curing time = 50–70 s.

2.5. Microstructure and property characterizations

Crystal structures of as-synthesized ZnO nanoparticles were characterized by an X-ray diffractometer (XRD, MacScience M18XHF) within Cu-K_α radiation (λ = 0.154 nm) at a scan rate of 4°/min. Absorption spectra of ZnO nanoparticles were recorded by UV–vis spectrophotometer (Hitachi 3900H). Photoluminescence (PL) spectrum of ZnO nanoparticles was obtained by a Hitachi F-4500 spectrophotometer. Fourier-transform infrared (FT-IR) spectra and nuclear-magnetic resonance spectra (^{1}H NMR) of ZnO nanoparticles prior to and after the surface modification by TPMA was characterized by a PerkinElmer spectrum 100 FT-IR spectrometer and a Varian Unity 300 MHz NMR spectrometer using DMSO-d_6 solvent, respectively. Microstructures of ZnO nanoparticles and ZnO-acrylic nanocomposites were examined by transmission electron microscopy (TEM, Philips Tecnai 20) operating at 200 kV. TEM sample of ZnO nanoparticles was prepared by spreading the samples on carbon-clad Cu meshes and, for ZnO-acrylic nanocomposites, their TEM samples were prepared by using the ultramicrotomy (Leica UltraCut E). The metal-insulator-metal (MIM) samples containing the ZnO-acrylic nanocomposites were prepared for the electrical property measurements. The top and bottom Ag electrodes were prepared by screen printing of Ag paste. After drying in vacuum for at least 24 h, the capacitances of MIM samples were measured by an HP 4194A gain/impedance analyzer operating in the frequencies ranging from 1.4 to 10 MHz and an

HP 4291B impedance analyzer operating in the frequencies ranging from 10 to 600 MHz, respectively. The relative dielectric constant (κ) was calculated according to the formula

$$\kappa = \frac{Ct}{\varepsilon_o A}, \quad (1)$$

where C = capacitance, ε_o = the vacuum dielectric permittivity, A = the area of electrode = 0.283 cm^2, and t = the thickness of cured nanocomposite layer = 300 μm.

3. Results and discussion

3.1. Characterizations of ZnO nanoparticles

Fig. 1 presents the UV–vis absorption profile of ZnO nanoparticles in ethanol solution. As shown in Fig. 1, distinct blue shift of absorption profile occurs in the ZnO nanoparticle sample as its absorption peak shifts to short wavelength side in comparison with that of bulk ZnO [25]. This is attributed to the quantum confinement effect caused by the size reduction of ZnO particles prepared in this work [24]. The data extracted from UV–vis absorption spectrum was also adopted to calculate the average size (d) of ZnO nanoparticles by using the expression as follows [24]:

$$\frac{1240}{\lambda_{0.5}} = 3.301 + \frac{294.0}{d^2} + \frac{1.09}{d}, \quad (2)$$

where $\lambda_{0.5}$ is the wavelength corresponding to the shoulder of absorption profile at half height of intensity. For the ZnO nanoparticles, $\lambda_{0.5}$ is about 350 nm and, according to Eq. (2), the average size of ZnO nanoparticles is about 3.75 nm.

The PL spectrum of ZnO nanoparticles shown in Fig. 2 depicts a strong emission peak with the maximum locating at the wavelength about 520 nm. Such a broad green-yellow emission is commonly ascribed to the recombination of electrons at the edge of conduction band (CB) or exciton states with the deeply trapped holes $V_O^{\bullet}/V_O^{\bullet\bullet}$ (2.0–2.2 eV below CB) in the bulk of ZnO quantum dots (QDs) [26–28]. This

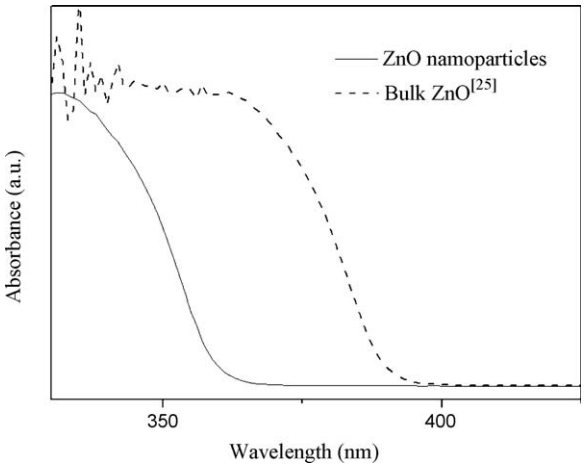

Fig. 1. UV-vis absorption profile of ZnO nanoparticles in ethanol solution and bulk ZnO. The profile for bulk ZnO is deduced from Ref. 25.

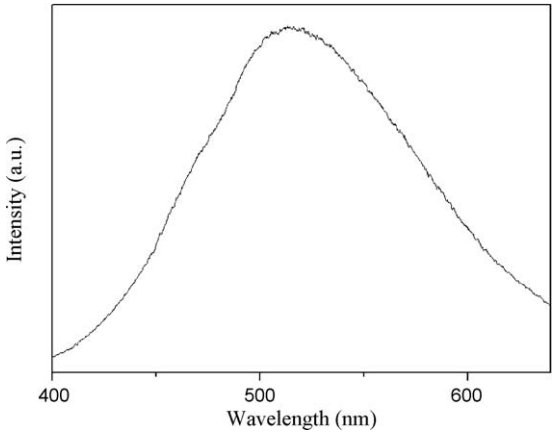

Fig. 2. PL spectrum of ZnO nanoparticles in ethanol solution.

implies the ZnO nanoparticles prepared in this work may abound with oxygen vacancies.

XRD pattern presented in Fig. 3 indicates the typical wurtzite structure of ZnO nanoparticles and the relatively broad diffraction peaks might be resulted from the size reduction effects as well as the abundance of lattice defects in ZnO. The average size of ZnO nanoparticles was calculated by using the Scherrer's formula [29] and was found to be about 3.8 nm. A high magnification TEM image of ZnO nanoparticles attached in Fig. 4 reveals that the size of ZnO nanoparticles is about 4 nm, evidencing the consistency of data presented above.

3.2. Surface modification of ZnO nanoparticles

Due to the presence of silane and acrylic functional groups in its molecular structure, TPMA was adopted to serve as the interfacial coupling agent as well as the dispersant of ZnO nanoparticles in polymeric matrix. Silane functional group may undergo chemical reactions to couple ZnO nanoparticles with acrylic matrix while the acrylic functional group provides the reaction sites with monomers *via* free-radical photo-polymerization so as to ensure the successful preparation of transparent ZnO-acrylic nanocomposites.

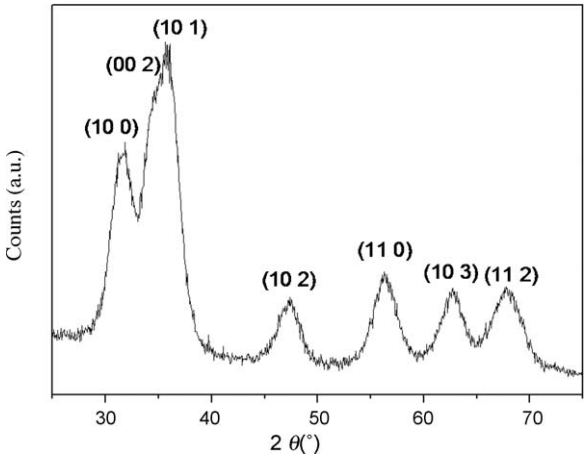

Fig. 3. XRD pattern of as-synthesized ZnO nanoparticles.

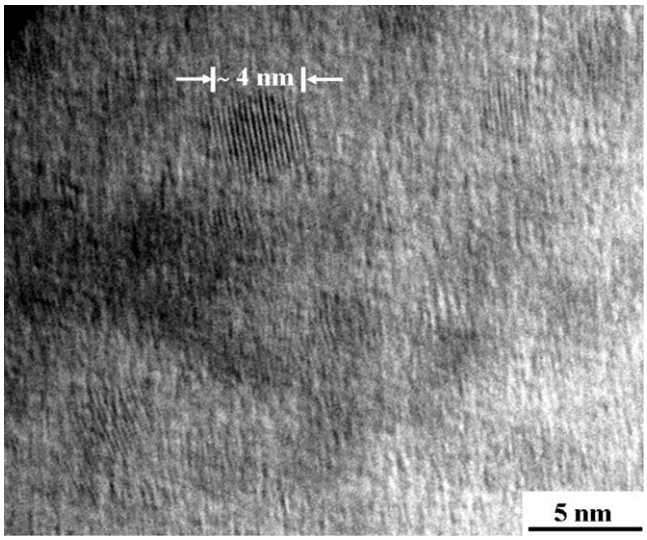

Fig. 4. Bright-field TEM micrograph of as-synthesized ZnO nanoparticles.

Fig. 5 shows the FT-IR spectra of as-synthesized ZnO nanoparticles and those subjected to surface modification by TPMA. The absorption bands at 1565 and 1420 cm^{-1} in both samples are assigned to the surface absorbed carboxylate anion complex [30] with the zinc center, indicating the chemical absorption of acetate group on the surface of ZnO. As to the TPMA-modified ZnO, the absorption bands corresponding to the Si–OH stretching vibration peak at 885 cm^{-1} and the Si–O–Si symmetrical stretching vibration peak at 1185 cm^{-1} [31] emerge, evidencing the successful attachment of TPMA on ZnO nanoparticle surface.

Fig. 6 presents the ^{1}H NMR spectra of TPMA, TPMA-modified and as-synthesized ZnO nanoparticles, respectively. In ^{1}H NMR spectrum for TPMA, the resonance peaks at 6.00 and 5.63 ppm are assigned to the methylene protons (peak H_2). The three resonance peaks at 4.02, 1.65, and 0.61 ppm are assigned to the α-CH_2, β-CH_2, and γ-CH_2 protons (peaks H_3, H_4, and H_5) of methacrylate, respectively. The resonance peak at 1.86 ppm is attributed to the proton of methyl group (peak H_1) near the methylene group and the resonance peak at

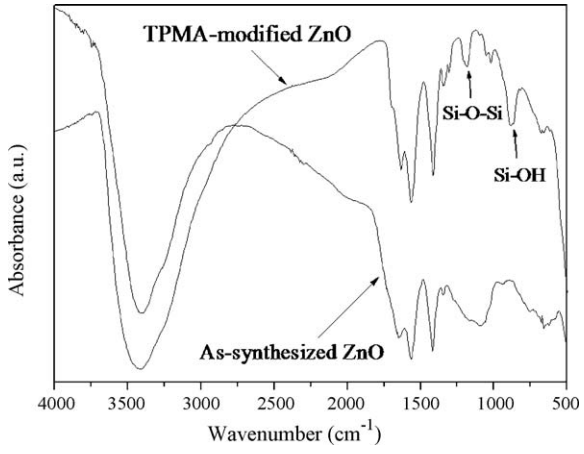

Fig. 5. FT-IR spectra of as-synthesized and TPMA-modified ZnO nanoparticles.

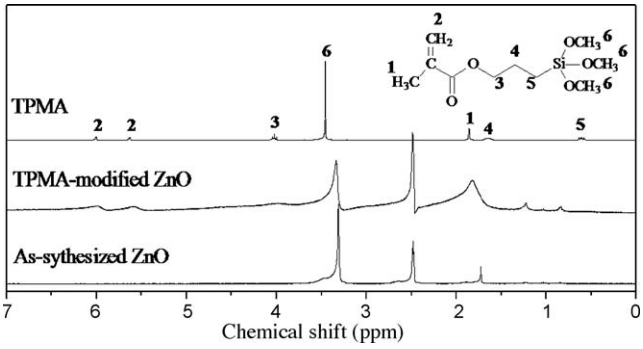

Fig. 6. ^{1}H NMR spectra of TPMA, TPMA-modified and as-synthesized ZnO nanoparticles.

3.45 ppm is ascribed to methyl protons of trimethylsilane (peak H_6). In ^{1}H NMR spectrum of as-synthesized ZnO nanocrystals, the peak of 1.73 ppm is resulted from the methyl proton of the acetate group which is in agreement with the FT-IR spectra presented in Fig. 5. The resonance peaks at 2.48 and 3.31 ppm are DMSO-d_6 and H_2O, respectively. A comparison of the ^{1}H NMR spectra of TPMA and TPMA-modified ZnO indicates the absence of H_6 peak and the significant broadening of H_1, H_2 and H_3 peaks in the TPMA-modified ZnO sample. The diminishing of H_6 peak in TPMA-modified ZnO nanoparticles is attributed to the hydrolysis–condensation reaction of TPMA bonded on ZnO particle surface. As to the broadening of H_1, H_2 and H_3 peaks, it is resulted from the inhomogeneity of the local chemical environment in the magnetic field [32]. When protons are attached the nanoparticle surface, in general the proton motion will be more strictly confined and hence the resonance peaks broaden. Analytical results of FT-IR and ^{1}H NMR spectra hence indicate that the TPMA is successfully bonded on ZnO particle surface by the hydrolysis–condensation reaction of trimethoxysilyl group in TPMA.

3.3. Characterizations of ZnO-acrylic nanocomposites

Fig. 7(a) and (b) respectively shows the UV–vis absorption spectra and appearances of pristine polymer and the nanocomposite samples containing 5, 10 and 20 *wt.%* TPMA-modified ZnO nanoparticles. Regardless of the amounts of filler loading, the transmittances of nanocomposite samples are very much the same as that of pristine polymer and they all exhibit high optical transmittances greater than 95% in visible light wavelengths from 400 to 800 nm. The intensity losses of incident light in a composite sample resulted from light scattering can be evaluated by using the following expression [33]:

$$\frac{I}{I_o} = \exp\left[-\frac{3V_{filler}xd^3}{32\lambda^4}\left(\frac{n_{filler}}{n_{matrix}} - 1\right)\right], \quad (3)$$

where I is the intensity of light passing through the specimen, I_0 is the intensity of incident light, d is the diameter of spherical filler particles with a refractive index n_{filler}, n_{matrix} is the refractive index of the matrix, V_{filler} is the volume fraction of filler particles, λ is the wavelength of incident light and x is

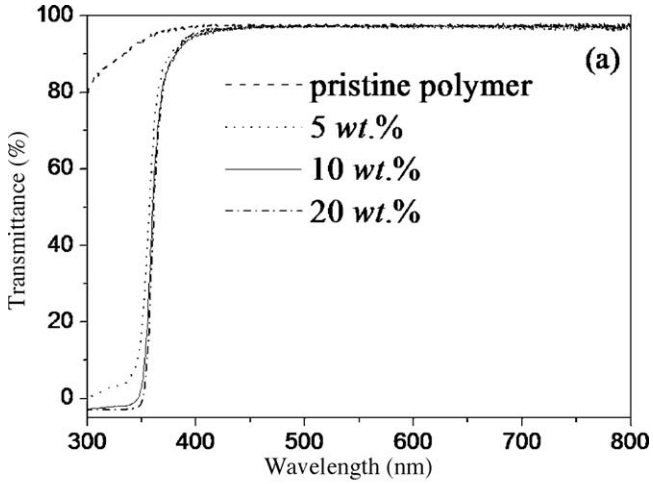

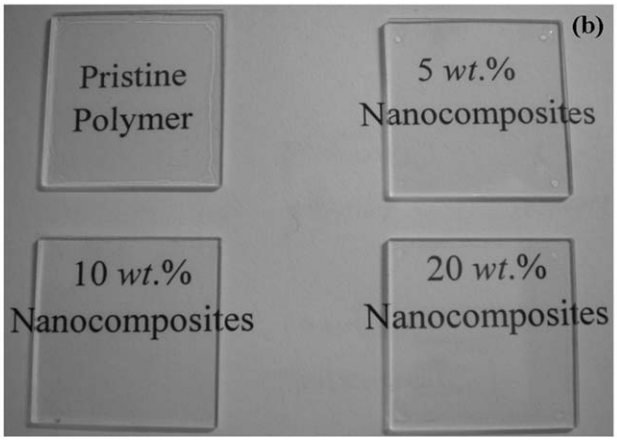

Fig. 7. (a) UV-vis spectra of pristine polymer and nanocomposite samples containing 5, 10 and 20 wt.% TPMA-modified ZnO nanoparticles. (b) Appearances of samples in (a) taken by digital camera. Thicknesses of samples are about 4 μm.

the optical path length. By substituting the values of $d \approx 4$ nm, $n_{filler} \approx 2$ for ZnO, $n_{matrix} \approx 1.45$ for acrylic and $x = 4$ μm into Eq. (3), it was found that the intensity loss of incident light is as low as 0.01% for the nanocomposite sample with $V_{filler} = 0.051$ (*i.e.*, the sample with 20 *wt.%* ZnO filler loading) at $\lambda = 600$ nm. Furthermore, Eq. (3) indicates that the aggregation of ZnO in polymer matrix would induce a dramatic intensity loss of transmitting light, *i.e.*, a suppression of transparency of ZnO-acrylic nanocomposites. As revealed by the analytical results shown in Fig. 7, the highly transparent feature of ZnO-acrylic nanocomposites with high-filler-loading hence indicates a uniform dispersion of ZnO nanoparticles in polymeric matrix. Such a fine dispersion behavior is evidenced by the TEM characterization of sample shown in Fig. 8. The results above hence illustrate the success on preparing the ZnO-acrylic nanocomposites by using TPMA to enhance the interfacial compatibility in between ZnO nanoparticles and acrylic monomers.

Fig. 9(a) and (b) separately presents the dielectric constants and dielectric losses of nanocomposites containing various amounts of ZnO nanoparticles measured in the frequency range of 1.0–600 MHz. As shown in Fig. 9(a), the UV-curable

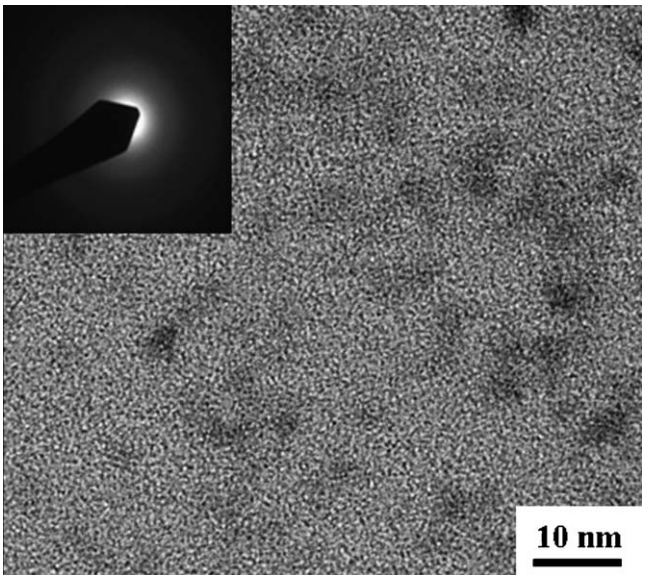

Fig. 8. Bright-field TEM micrograph of ZnO-acrylic nanocomposite containing 20 wt.% of TPMA-modified ZnO nanoparticles.

nanocomposite thin films with dielectric constants greater than 4 can be achieved. Further, it can be seen that both the dielectric constant and dielectric loss of nanocomposites increase with the increase of ZnO content. Implantation of ZnO nanoparticles in

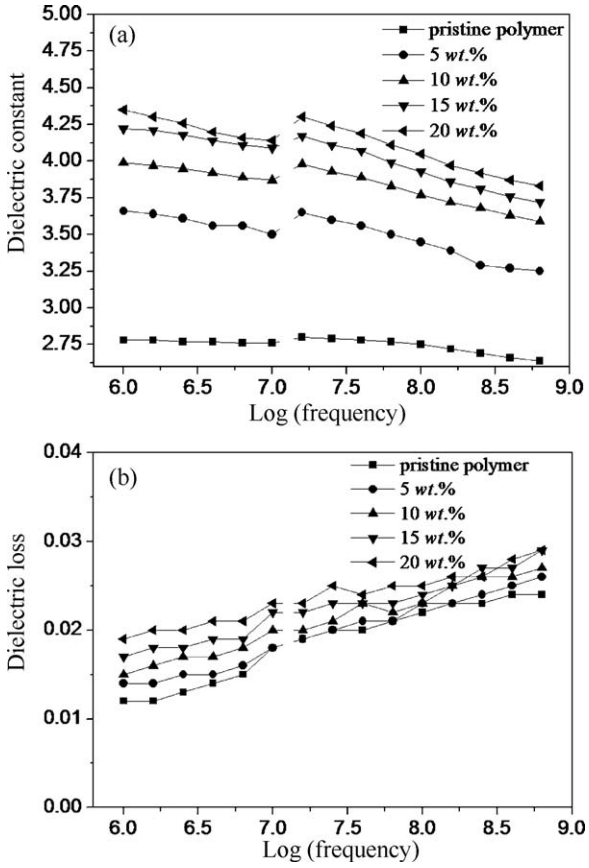

Fig. 9. (a) Dielectric constant and (b) dielectric loss of ZnO-acrylic nanocomposites as a function of measuring frequency. The data discontinuities at 10 MHz were resulted from the difference in measuring frequency ranges of HP4194A and HP 4291B impedance analyzers.

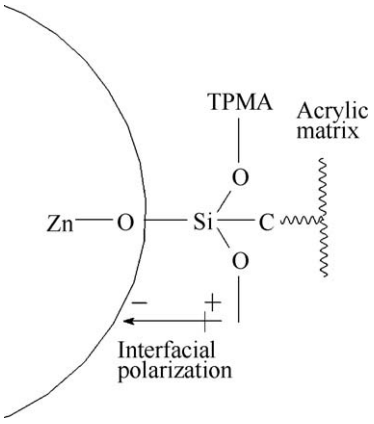

Fig. 10. Schematic illustration of the interfacial polarization at ZnO/acrylic interface.

acrylic matrix results in a substantial improvement of dielectric constant without dramatic deterioration of dielectric loss. For instance, at 1 MHz an increase of dielectric constant from 2.8 to about 4.35 (about 55% enhancement) with dielectric loss less than 0.02 can be obtained in the nanocomposite containing 20 *wt.%* inorganic filler. Such a highly transparent thin film with good flatness possesses promising applications, *e.g.*, the gate dielectric of OTFTs or the encapsulation layer for flexible organic electronic devices.

Table 1 lists the comparison of dielectric constants obtained by experimental measurement and theoretical calculation in terms of the Maxwell–Garnett effective medium approximation [34]. As shown in Table 1, the experimental values are always higher than the theoretical calculated values. Previous studies reported that interfacial interactions may affect the dielectric properties of composites [35–41]. Since Maxwell–Garnett approximation is applied to homogeneous composites containing spherical filler particles without considering the interactions in between the filler and polymer phases, it hence is speculated that interfacial polarization may contribute to the dielectric constant enhancement of nanocomposites. In our nanocomposite samples, interfacial polarization may be resulted from the interactions between the silane functional group in the branch of acrylic polymer and ZnO nanoparticles as illustrated in Fig. 10. Further, the size reduction of filler particles to nanometer scale drastically escalates the specific surface area (SSA) of ZnO and thus amplifies the contribution of interfacial polarization on dielectric constant property of nanocomposites.

Finally, Fig. 9(a) also shows that the increasing trend of dielectric constant gradually alleviates with the increase of ZnO content in nanocomposite samples. High inorganic filler loading may cause scattering/reflection of UV light which, in turn, results in the incomplete photo-curing and thus the physical property degradation of UV-curable nanocomposites. In order to complete the photo-curing, a prolonged UV exposure is required for high-filler-loading samples. Nevertheless, it might cause excessive photo-curing and induce the oxidation of polymer component in nanocomposites. It is speculated that photo-induced oxidation may be the cause of alleviation of dielectric constant increment as shown in Fig. 9(a) and, hence, there is a limit of inorganic filler loading when preparing the UV-curable nanocomposites.

Table 1
A list of calculated and measured dielectric constants of nanocomposites.

Sample	ZnO content (*wt.%*)	Calculated value[a]	Experimental value[b]
Pristine polymer	0	2.78	2.78
Nanocomposites	5	2.82	3.66
	10	2.86	3.99
	15	2.91	4.22
	20	2.96	4.35

[a] Theoretical dielectric constants of nanocomposites, ε_{com}, were calculated in terms of Maxwell-Garnett effective medium approximation [33], $\varepsilon_{com} = \varepsilon_m \frac{\varepsilon_f + 2\varepsilon_m + 2f(\varepsilon_f - \varepsilon_m)}{\varepsilon_f + 2\varepsilon_m - f(\varepsilon_f - \varepsilon_m)}$, where ε_m = dielectric constant of acrylic matrix = 2.78, ε_f = dielectric constant of wurtzite ZnO = 8.75 and f = the volume fraction of ZnO filler.

[b] Experimental values were obtained at 1 MHz.

4. Conclusions

This study demonstrates the preparation of ZnO nanoparticles and UV-curable ZnO-acrylic nanocomposites containing the TPMA-modified ZnO nanoparticles. Analytical results indicated that the sol–gel chemical route employed in this study successfully produces the ZnO particles as small as 4 nm. A fine dispersion of filler particles in polymeric matrix was achieved *via* the surface modification with TPMA which serves both as the interfacial coupling agent and dispersant of ZnO nanoparticles in acrylic matrix. UV–vis characterization revealed a high optical transparency (>95%) in visible light region for nanocomposites with ZnO content as high as 20 *wt.%*. Electrical measurement indicated that the addition of ZnO nanoparticles in acrylic matrix enhances the dielectric constants of nanocomposite thin films and the dielectric constants exceeding 4 could be achieved in the samples with ZnO contents higher than 10 *wt.%*. A comparison of experimental values and theoretical calculation implied that interfacial polarizations may also contribute the dielectric constant enhancement since the scaled-down of ZnO particle size to nanometer scale effectively increases the SSA of ZnO.

Acknowledgement

This work is supported by the National Science Council (NSC) of the Republic of China under the contract NSC95-2221-E009-130.

References

[1] J. Golebiewski, A. Galeski, Thermal stability of nanoclay polypropylene composites by simultaneous DSC and TGA, Compos. Sci. Technol. 67 (15–16) (2007) 3442–3447.
[2] T.H. Chiang, S.L. Liu, S.Y. Lee, T.E. Hsieh, Preparation, microstructure, and property characterizations of fluorinated polyimide–organosilicate hybrids, Eur. Polym. J. 44 (11) (2008) 3482–3492.
[3] S.P. Mondal, V.S. Reddy, S. Das, A. Dhar, S.K. Ray, Memory effect in a junction-like CdS nanocomposite/conducting polymer Poly[2-methoxy-5-

(2-ethylhexyloxy)-1,4-phenylene-vinylene] heterostructure, Nanotechnology 19 (21) (2008) 15306–215309.
[4] J. Xu, J. Wang, M. Mitchell, P. Mukherjee, M. Jeffries-EL, J.W. Petrich, Z. Lin, Organic–inorganic nanocomposites via directly grafting conjugated polymers onto quantum dots, J. Am. Chem. Soc. 129 (42) (2007) 12828–12833.
[5] C.L. Lu, Z.C. Cui, Y. Wang, Z. Li, C. Guan, B. Yang, J.C. Shen, Preparation and characterization of ZnS–polymer nanocomposite films with high refractive index, J. Mater. Chem. 13 (9) (2003) 2189–2195.
[6] V. Khrenov, M. Klapper, M. Koch, K. Müllen, Surface functionalized ZnO particles designed for the use in transparent nanocomposites, Macromol. Chem. Phys. 206 (1) (2005) 95–101.
[7] S.H. Stelzig, M. Klapper, K. Müllen, A simple and efficient route to transparent nanocomposites, Adv. Mater. 20 (5) (2008) 929–932.
[8] H. Althues, R. Palkovits, A. Rumplecker, P. Simon, W. Sigle, M. Bredol, U. Kynast, S. Kaskel, Synthesis and characterization of transparent luminescent ZnS:Mn/PMMA nanocomposites, Chem. Mater. 18 (4) (2006) 1068–1072.
[9] C.L. Lu, C. Guan, Y.F. Liu, Y.R. Cheng, B. Yang, PbS/polymer nanocomposite optical materials with high refractive index, Chem. Mater. 17 (9) (2005) 2448–2454.
[10] Y. Yang, Y.Q. Li, S.Y. Fu, H.M. Xiao, Transparent and light-emitting epoxy nanocomposites containing ZnO quantum dots as encapsulating materials for solid state lighting, J. Phys. Chem. C 112 (28) (2008) 10553–10558.
[11] Y.Y. Wang, T.E. Hsieh, I.C. Chen, C.H. Chen, Direct encapsulation of organic light emitting devices (OLEDs) using photo-curable co-polyacrylate/silica nanocomposite resin, IEEE T. Adv. Packaging 30 (3) (2007) 421–427.
[12] Y.G. Seol, J.G. Lee, N.E. Lee, Effects of different electroplated gate electrodes on electrical performances of flexible organic thin film transistor and flexibility improvement, Org. Electron. 8 (5) (2007) 513–521.
[13] C.Y. Jiang, X.W. Sun, K.W. Tan, G.Q. Lo, A.K.K. Kyaw, D.L. Kwong, High-bendability flexible dye-sensitized solar cell with a nanoparticle-modified ZnO-nanowire electrode, Appl. Phys. Lett. 92 (14) (2008) 143101–143103.
[14] D.C. Reynold, D.C. Look, B. Jogai, H. Morkoc, Similarities in the bandedge and deep-centre photoluminescence mechanisms of ZnO and GaN, Solid State Commun. 101 (9) (1997) 643–646.
[15] Y.Y. Peng, T.E. Hsieh, C.H. Hsu, Optical characteristics and microstructure of ZnO quantum dots-SiO_2 nanocomposite films prepared by sputtering methods, Appl. Phys. Lett. 89 (21) (2006) 211909–211911.
[16] S. Chakrabarti, D. Das, D. Ganguli, S. Chaudhuri, Tailoring of room temperature excitonic luminescence in sol–gel zinc oxide–silica nanocomposite films, Thin Solid Films 441 (1–2) (2003) 228–237.
[17] H. He, Y. Wang, Y. Zou, Photoluminescence property of ZnO–SiO_2 composites synthesized by sol–gel method, J. Phys. D 36 (23) (2003) 2972–2975.
[18] L. Guo, S. Yang, C. Yang, P. Yu, J. Wang, W. Ge, K.L. Wong, Highly monodisperse polymer-capped ZnO nanoparticles: preparation and optical properties, Appl. Phys. Lett. 76 (20) (2000) 2901–2903.
[19] R. Viswanatha, S. Sapra, B. Satpati, P.V. Satyam, B.N. Dev, D.D. Sarma, Understanding the quantum size effects in ZnO nanocrystals, J. Mater. Chem. 14 (4) (2004) 661–668.
[20] Y.Y. Peng, T.E. Hsieh, C.H. Hsu, White-light emitting ZnO–SiO_2 nanocomposite thin films prepared by the target-attached sputtering method, Nanotechnology 17 (1) (2006) 174–180.
[21] A. van Dijken, E.A. Meulenkamp, D. Vanmaekelbergh, A. Meijerink, The luminescence of nanocrystalline ZnO particles: the mechanism of the ultraviolet and visible emission, J. Lumin. 87–89 (2000) 454–456.
[22] M.A. Reshchikov, H. Morkoc, B. Nemeth, J. Nause, J. Xie, B. Hertog, A. Osinsky, Luminescence properties of defects in ZnO, Physica B 401–402 (2007) 358–361.
[23] I.W. Mikrajuddin, K. Lenggoro, F.G. Okuyama, Shib, Luminescent polymer electrolytes prepared by growing ZnO nanoparticles in the matrix of polyethylene glycol, J. Electrochem. Soc. 149 (5) (2002) H107–H112.
[24] E.A. Meulenkamp, Synthesis and growth of ZnO nanoparticles, J. Phys. Chem. B 102 (29) (1998) 5566–5572.
[25] M. Bouloudenine, N. Viart, S. Colis, J. Kortus, A. Dinia, Antiferromagnetism in bulk $Zn_{1-x}Co_xO$ magnetic semiconductors prepared by the coprecipitation technique, Appl. Phys. Lett. 87 (5) (2005) 052501–052503.
[26] K. Vanheusden, W.L. Warren, C.H. Seager, D.R. Tallant, J.A. Voigt, Mechanisms behind green photoluminescence in ZnO phosphor powders, J. Appl. Phys. 79 (10) (1996) 7983–7990.
[27] X.L. Wu, G.G. Siu, C.L. Fu, H.C. Ong, Photoluminescence and cathodoluminescence studies of stoichiometric and oxygen-deficient ZnO films, Appl. Phys. Lett. 78 (16) (2001) 2285–2287.
[28] S.U. Yuldashev, G.N. Panin, S.W. Choi, V.S. Yalishev, L.A. Nosova, M.K. Ryu, S. Lee, M.S. Jang, K.S. Chung, T.W. Hang, Electrical and optical properties of ZnO films grown on GaAs substrates, Jpn. J. Appl. Phys. 42 (2003) 3333–3336.
[29] B.D. Cullity, S.R. Stock, Elements of X-ray Diffraction, 3rd, 2001.
[30] S. Sakohara, M. Ishida, M.A. Anderson, Visible luminescence and surface properties of nanosized ZnO colloids prepared by hydrolyzing zinc acetate, J. Phys. Chem. B 102 (50) (1998) 10169–10175.
[31] X.Y. Shang, Z.K. Zhu, J. Yin, X.D. Ma, Compatibility of soluble polyimide/silica hybrids induced by a coupling agent, Chem. Mater. 14 (1) (2002) 71–77.
[32] Z. Chen, Z.W. Chen, J.H. Zhong, High-resolution NMR spectra in inhomogeneous fields via IDEAL (Intermolecular Dipolar-Interaction Enhanced All Lines) method, J. Am. Chem. Soc. 126 (2) (2004) 446–447.
[33] B.M. Novak, Hybrid nanocomposite materials between inorganic glasses and organic polymers, Adv. Mater. 5 (6) (1993) 422–433.
[34] A. Sihvola, Electromagnetic Mixing Formulas and Applications, London, 1999.
[35] W.F. Su, J.F. Lee, M.Y. Chen, R.M. Ho, Bismuth titanate nanoparticles dispersed polyacrylates, J. Mater. Res. 19 (8) (2004) 2343–2348.
[36] H.T. Vo, F.G. Shi, Towards model-based engineering of optoelectronic packaging materials: dielectric constant modeling, Microelectron. J. 33 (5–6) (2002) 409–415.
[37] P. Murugaraj, D. Mainwaring, N. Mora-Huertas, Dielectric enhancement in polymer nanoparticle composites through interphase polarizability, J. Appl. Phys. 98 (5) (2005) 054304–054309.
[38] K.S. Deepa, M.T. Sebastian, J. James, Effect of interparticle distance and interfacial area on properties of insulator–conductor composites, Appl. Phys. Lett. 91 (20) (2007) 202904–202906.
[39] M.G. Todd, F.G. Shi, Characterizing the interphase dielectric constant of polymer composite materials: effect of chemical coupling agents, J. Appl. Phys. 94 (7) (2003) 4551–4557.
[40] Z.M. Dang, D. Xie, C.Y. Shi, Theoretical prediction and experimental study of dielectric properties in poly(vinylidene fluoride) matrix composites with micronanosize $BaTiO_3$ filler, Appl. Phys. Lett. 91 (22) (2007) 222902–222904.
[41] Z.M. Dang, H.P. Xu, H.Y. Wang, Significantly enhanced low-frequency dielectric permittivity in the $BaTiO_3$/poly(vinylidene fluoride) nanocomposite, Appl. Phys. Lett. 90 (1) (2007) 012901–012903.